frontiers in Chemistry

ORIGINAL RESEARCH
published: 05 December 2019
doi: 10.3389/fchem.2019.00775

Peroxynitrite Activated Drug Conjugate Systems Based on a Coumarin Scaffold Toward the Application of Theranostics

Maria L. Odyniec[1], Hai-Hao Han[2], Jordan E. Gardiner[1], Adam C. Sedgwick[3], Xiao-Peng He[2], Steven D. Bull[1]* and Tony D. James[1]**

[1] Department of Chemistry, University of Bath, Bath, United Kingdom, [2] Key Laboratory for Advanced Materials and Feringa Nobel Prize Scientist Joint, Research Center, East China University of Science and Technology, Shanghai, China, [3] Department of Chemistry, University of Texas at Austin, Austin, TX, United States

OPEN ACCESS

Edited by:
Tsuyoshi Minami,
University of Tokyo, Japan

Reviewed by:
Shunsuke T. Tomita,
National Institute of Advanced Industrial Science and Technology (AIST), Japan
Yuanli Liu,
Guilin University of Technology, China

***Correspondence:**
Maria L. Odyniec
m.l.odyniec@bath.ac.uk
Steven D. Bull
s.d.bull@bath.ac.uk
Tony D. James
t.d.james@bath.ac.uk

Specialty section:
This article was submitted to Supramolecular Chemistry, a section of the journal Frontiers in Chemistry

Received: 28 August 2019
Accepted: 25 October 2019
Published: 05 December 2019

Citation:
Odyniec ML, Han H-H, Gardiner JE, Sedgwick AC, He X-P, Bull SD and James TD (2019) Peroxynitrite Activated Drug Conjugate Systems Based on a Coumarin Scaffold Toward the Application of Theranostics. Front. Chem. 7:775. doi: 10.3389/fchem.2019.00775

Two novel drug-conjugates based on a "coumarin linker" have been designed for the synergic release of a therapeutic agent and fluorescent probe for the potential application of theranostics. The drug conjugates; **CC-RNS** and **CI-RNS** were designed to be activated by reactive oxygen species or reactive nitrogen species (ROS/RNS). The fluorescence OFF-ON response was triggered by the peroxynitrite-mediated transformation of a boronic acid pinacol ester to a phenol moiety with simultaneous release of the therapeutic agents (Confirmed by HRMS). The limit of detection for peroxynitrite using **CC-RNS** and **CI-RNS** was 0.29 and 37.2 μM, respectively. Both **CC-RNS** and **CI-RNS** demonstrated the ability to visualize peroxynitrite production thus demonstrating the effectiveness of these probes for use as tools to monitor peroxynitrite-mediated drug release in cancer cell lines.

Keywords: theranostic, peroxynitrite, coumarin, chemosensor, fluorescence

INTRODUCTION

Theranostic systems, are the combination of a diagnostic and therapeutic and represent an emerging area with regard to effective cancer treatment. There have been an increasing number of examples of small-molecule theranostics which have good selectivity and high anti-tumor activity (Aulic et al., 2013; Kumar et al., 2015). In this respect, new theranostic probes are required for whole organism fluorescence tumor imaging and image guided surgery (Blau et al., 2018).

Real time monitoring of drug action is a prime concern for target specific cancer treatment. Redox-responsive chemotherapy is gaining attention. In such cases, a chemotherapeutic molecule is commonly attached to a fluorophore *via* a sacrificial self immolative linker (i.e., disulphide) (Wu et al., 2014; Gangopadhyay et al., 2017). Disulphide linkages are selectively cleaved in cancer cells by biological reducing agents, including glutathione (GSH); owing to high levels in cellular environments (2–10 mM) (Lu, 2013). Other examples of theranostic systems include hypoxia-induced and hydrogen peroxide activatable self-immolative systems (Kumar et al., 2014, 2016).

A potential problem for "multi-component" systems is that the chromophore and therapy module could be released independently. One method to circumvent this problem is to use the fluorophore as the "linker" which can be functionalized with both an activating group

and a therapeutic. In seminal work, Shabat et al. designed a theranostic prodrug using a self-immolative coumarin linker (**Figure 1**). The drug-delivery system uses a 7-hydroxycoumarin with a hydroxymethyl substituent. The phenolic alcohol of 7-hydroxycoumarin is linked to an activating group and the hydroxymethyl substituent acts as an attachment point for a drug or targeting group. In this example; **Cou-Melphalan** incorporates melphalan as a therapeutic with attachments *via* carbamates. This theranostic was designed to be activated by Cathespin B (Weinstain et al., 2013).

We were interested in utilizing the "coumarin linker" since they are natural products with simple preparative routes. Coumarin has important biological activities including; anti-tumor, anti-HIV and anti-bacterial properties, with multiple coumarin-derived molecules reported to cross the blood brain barrier (Borges et al., 2005; Yang et al., 2015). Various activating mechanisms for theranostics have been used; including activation by reactive oxygen species (ROS), intracellular thiols and enzymes (Chan et al., 2012). The reactive nitrogen species (RNS), peroxynitrite ($ONOO^-$) is of interest due to its orthogonal reactivity with boronate esters and increased reactivity compared to its equivalent reactive oxygen species (ROS), hydrogen peroxide (H_2O_2) (Sedgwick et al., 2016, 2017; Wu et al., 2018). To this end, we set out to design $ONOO^-$ activatable systems (**Figure 2**) (Yang et al., 2006; Sedgwick et al., 2016, 2018). The probes **CI-RNS** and **CC-RNS** were designed with ester linkers, in order to determine whether the same 1–8 self-immolative effect can occur, as in Shabat's system. Since, the use of an ester attachment provides access to probe-based systems using simpler synthetic procedures (Weinstain et al., 2013). The proposed disassembly mechanism is illustrated in **Scheme 1**.

In vivo $ONOO^-$ is generated through the diffusion limited reaction of superoxide ($O_2^{\bullet-}$) and nitric oxide (NO). Both $O_2^{\bullet-}$ and NO are non-toxic *in vivo* due to efficient methods to minimize accumulation (Beckman, 1996). Under proinflammatory conditions, production of $O_2^{\bullet-}$ and NO is activated, which inevitably increases the concentration of $ONOO^-$ (Pacher et al., 2007). Typically, *in vitro* studies, the concentration of $ONOO^-$ is enhanced by the $ONOO^-$ donor SIN1 or stimulation of an inflammatory response using LPS and IFN-γ. The repurposing of the boronate-based probe peroxyresorufin-1 (PR1) Miller et al. (2005) to detect $ONOO^-$ *in vitro* using these methods was reported by Weber et al. (2018). Interestingly, there is no reported data for loss of drug function through reaction with $ONOO^-$. Examples of drug delivery systems which are activated by H_2O_2 have shown that, on release of the drug, the drug released still has the desired therapeutic response (Kumar et al., 2014; Wang et al., 2017).

As therapeutic payloads we chose; chlorambucil and indomethacin, providing distinct mechanisms of action for our theranostic probes. Chlorambucil is a DNA alkylating agent from the nitrogen mustard family. It is used to treat leukemia, Hodgkin's disease and non-Hodgkin lymphomas (Begleiter et al., 1996). Nitrogen mustards are generally unstable (Wang et al., 2010). Off-target reactions with proteins and biological thiols reduce drug potency, requiring higher dosages to produce a substantial therapeutic response. The repurposing and targeting of chlorambucil to enhance treatment scenarios are currently

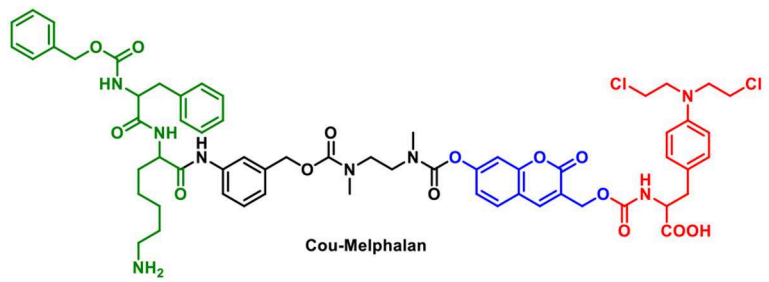

FIGURE 1 | Structure of **Cou-Melphalan**.

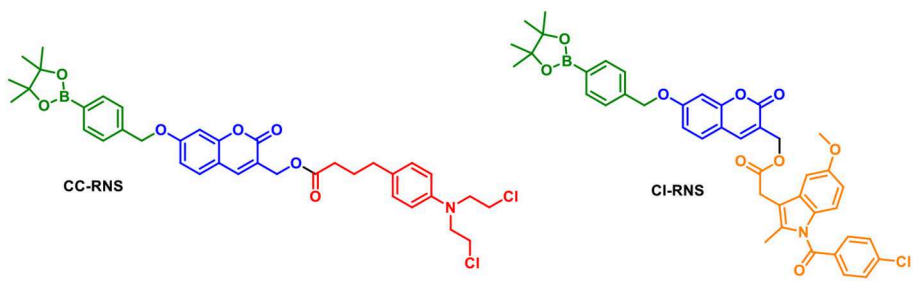

FIGURE 2 | Structures of **CC-RNS** and **CI-RNS**.

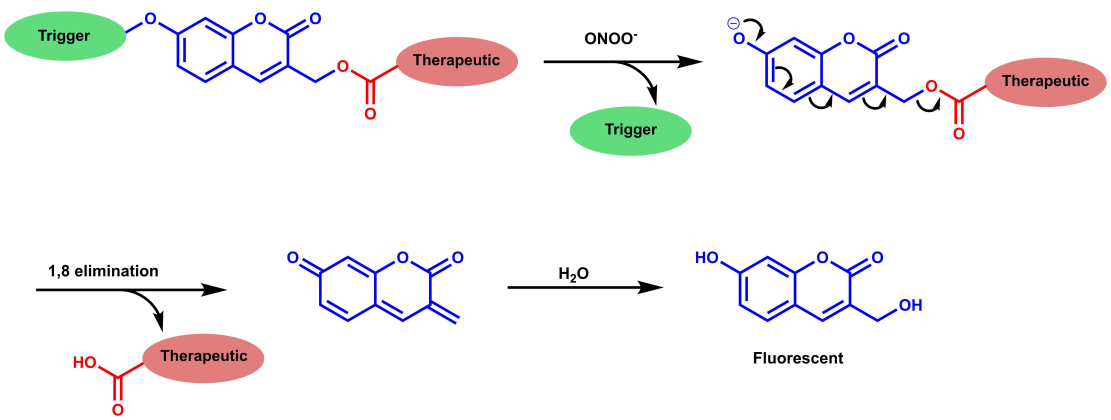

SCHEME 1 | Proposed disassembly mechanism of **CC-RNS** and **CI-RNS**, adapted from Weinstain et al. (2013).

being investigated with successful preliminary studies in breast and pancreatic cancer cell lines (Millard et al., 2013; Kaur et al., 2017).

Indomethacin is primarily a non-steroidal anti-inflammatory drug (NSAID). Indomethacin inhibits the cyclooxygenase enzymes which catalyze the production of prostaglandins; responsible for inflammation and pain (Lucas, 2016). More recently; the effect of indomethacin on the modulation of the inflammatory responses in cancer have been investigated. Indomethacin has been shown to reduce cell migration, invasion, and metastasis in breast and colon cancer cell lines (Ackerstaff et al., 2007; Guo et al., 2013).

RESULTS AND DISCUSSION

CI-RNS and **CC-RNS** were synthesized according to **Scheme 2**. **CI-RNS** was prepared over seven steps. **CC-RNS** was synthesized in six steps. First, coumarin-derivative (**4**) was obtained using previous literature procedures (Kim et al., 2014; Behara et al., 2017). Coumarin (**1**) was obtained by reacting 2,4-dihydroxybenzaldehyde with propionic anhydride in the presence of sodium propionate and piperidine. Compound **1** subsequently underwent radical bromination to afford compound **2**; which was transformed into compound **3** *via* acetylation. Compound **3** was deprotected with potassium carbonate in MeOH to yield coumarin (**4**). 4-(Bromomethyl)phenylboronic acid pinacol ester was added to compound **4** in an alkylation reaction to produce compound **5** in moderate yield. To generate **CI-RNS**; compound **5** underwent bromination in the presence of PBr_3 to produce **6**. Thereafter, **CI-RNS** was obtained by reacting indomethacin in the presence of potassium carbonate, to afford the desired compound in 17% yield. To prepare **CC-RNS**; compound **5** was reacted with indomethacin using a HATU cross coupling reaction. This reaction gave the desired compound in a 9% yield.

Intermediate compound **5** is an example of a $ONOO^-$ activatable molecular probe. Therefore, the reactivity of **5** with $ONOO^-$ was investigated. All measurements were recorded in a PBS buffer solution (pH = 7.3) at ambient temperature. The measurements were recorded instantly after $ONOO^-$ addition. There is no change in UV-VIS absorption maximum at 315 nm on the addition of $ONOO^-$ (20 μM) to the probe **5** (20 μM) (**Supplementary Figure 1**). The fluorescence spectra of probe **5** (10 μM), shows a ratiometric response. With increasing concentrations of $ONOO^-$ (0–20 μM), there is a decrease in peak at 390 nm and emergence of a new peak at 460 nm; characteristic of free coumarin (**Figure 3**, **Supplementary Figure 2**). The limit of detection for **5** was calculated to be 76.5 nM (**Supplementary Figure 3**). The formation of free coumarin was also supported by mass spectroscopic studies; finding $[M]^-$ = 192.0417 (**Supplementary Figure 4**).

The spectroscopic properties of intermediate **6** were also investigated. 4-bromoumbelliferone shows weak fluorescence at 438 nm, therefore **6** is expected to be non-fluorescent (Thasnim and Bahulayan, 2017). This is due to the less electron-donating effect of the bromomethyl group compared to the methyl alcohol. Addition of $ONOO^-$ results in formation of 3-(bromomethyl)-7-hydroxy-2*H*-chromen-2-one; this is confirmed by mass spectroscopic analysis; where exact mass for $C_{10}H_7BrO_3$ $[M]^-$ = 253.9597 finds $[M]^-$ = 253.9569 (**Supplementary Figure 5**). There is no change in the UV-Vis response with absorption maxima at 340 nm (**Supplementary Figure 6**). Fluorescence studies carried out in PBS buffer pH = 7.3 at ambient temperature shows that **6** has a fluorescence emission at 390 nm. On addition of $ONOO^-$ (0–20 μM) there is a decrease in emission at 390 nm and increase in a new emission peak at 455 nm (**Figure 4**, **Supplementary Figure 7**). The limit of detection for **6** was calculated to be 54.6 nM (**Supplementary Figure 8**).

With probes **CC-RNS** and **CI-RNS** in hand, spectroscopic evaluations were performed. All measurements were recorded in PBS buffer solution (pH = 7.3) at ambient temperature. The measurements were recorded instantly after $ONOO^-$ addition. The UV-VIS spectrum of probe **CC-RNS** (20 μM) and **CI-RNS** (20 μM) were recorded with and without $ONOO^-$ (50 μM—**Supplementary Figures 9, 10**). From the UV-VIS

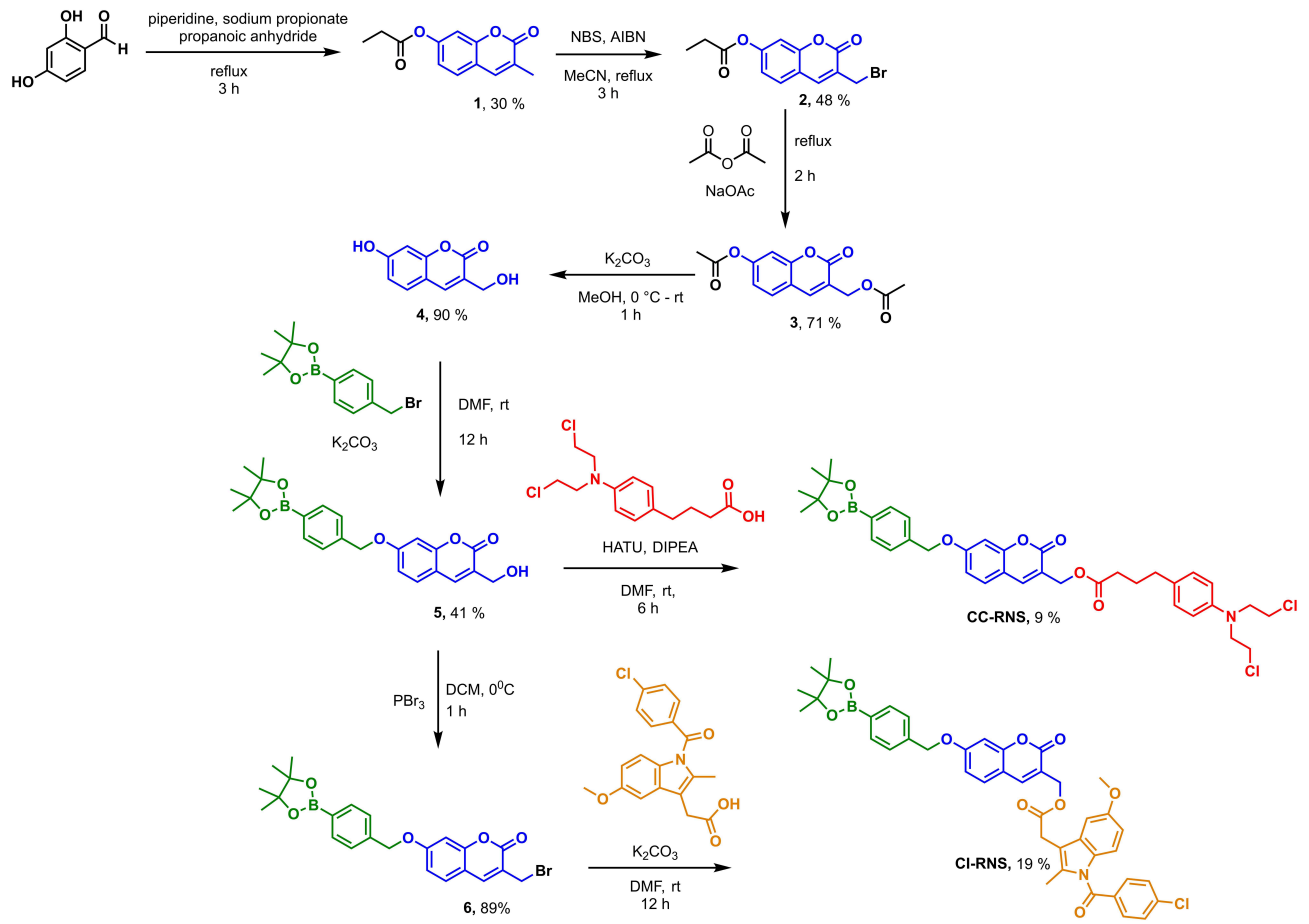

SCHEME 2 | Synthesis scheme of **CI-RNS** and **CC-RNS**.

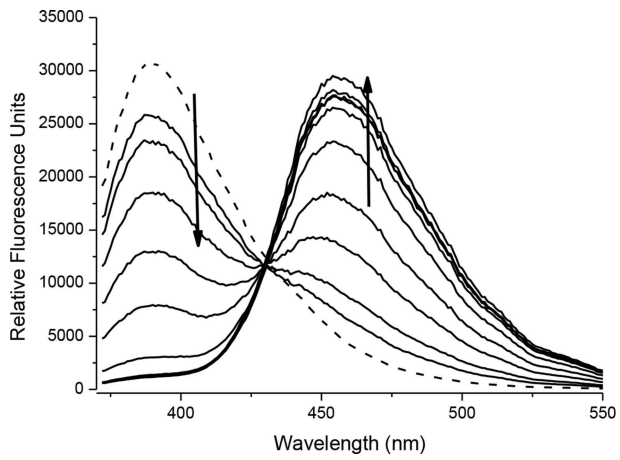

FIGURE 3 | Fluorescence spectra of **5** (10 μM) in the presence of $ONOO^-$ (0, 2, 4, 6, 8, 10, 12, 14, 16, 18, 20 μM). The data was collected in PBS buffer, pH = 7.3 at 25°C where λ_{ex} = 345 (16 bandwidth) nm. The dotted line represents probe only.

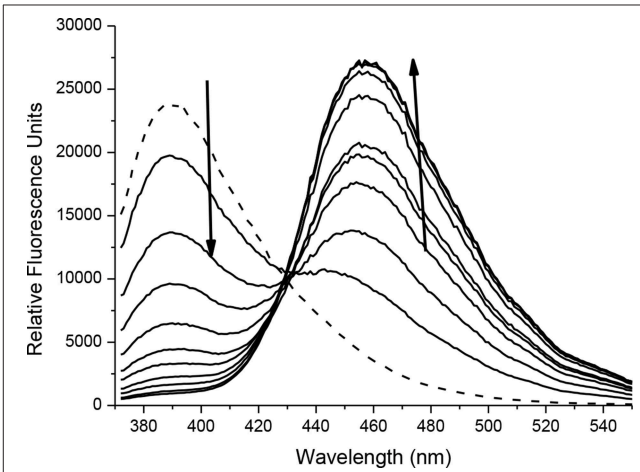

FIGURE 4 | Fluorescence spectra of **6** (10 μM) in the presence of $ONOO^-$ (0, 2, 4, 6, 8, 10, 12, 14, 16, 18, 20 μM). The data was collected in PBS buffer, pH = 7.3 at 25°C where λ_{ex} = 345 (16 bandwidth) nm. The dotted line represents probe only.

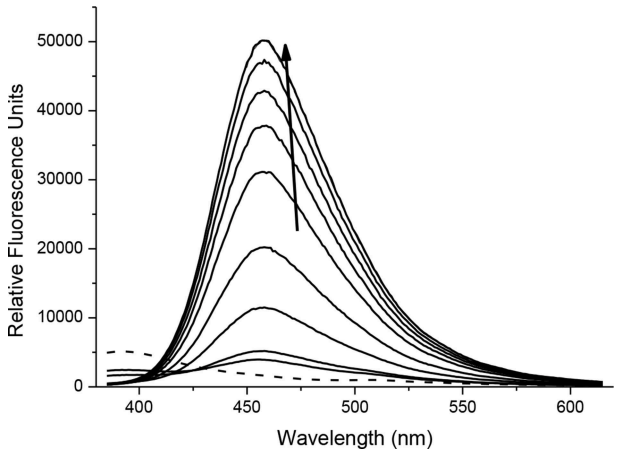

FIGURE 5 | Fluorescence spectra of **CC-RNS** (10 μM) in the presence of $ONOO^-$ (0–20 μM) in PBS buffer pH = 7.3. The data was collected at 25°C instantly after addition of peroxynitrite, where λ_{ex} = 345 (16 bandwidth) nm. The dotted line represents probe only.

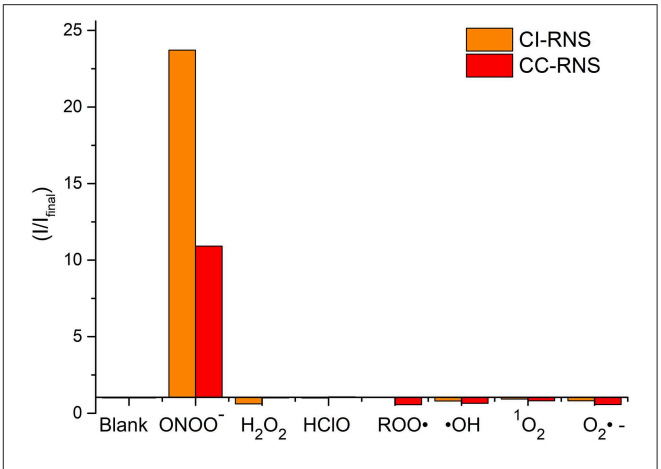

FIGURE 7 | Selectivity data of **CC-RNS** and **CI-RNS** (10 μM) in the presence of $ONOO^-$ (20 μM), H_2O_2 (200 μM), ClO^- (200 μM), ROO· (200 μM), OH (200 μM), $O_2^{\bullet-}$ (200 μM), and $^1O_2$ (200 μM) in PBS buffer pH = 7.3. The data was collected at 25°C after incubation for 15 min, where λ_{ex} = 345 (16 bandwidth) nm. Fluorescence intensity points were taken at λ_{max} = 460 nm.

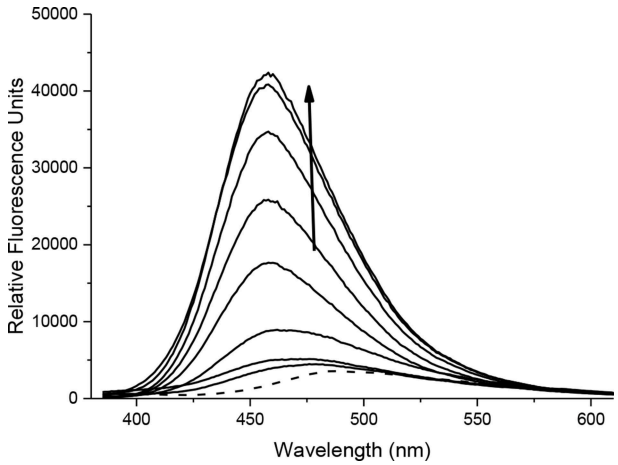

FIGURE 6 | Fluorescence spectra of **CI-RNS** (10 μM) in the presence of $ONOO^-$ (0, 10, 20, 25, 30, 35, 40, 45, 50 μM). The data was collected in PBS buffer, pH = 7.3 at 25°C where λ_{ex} = 345 (16 bandwidth) nm. The dotted line represents probe only.

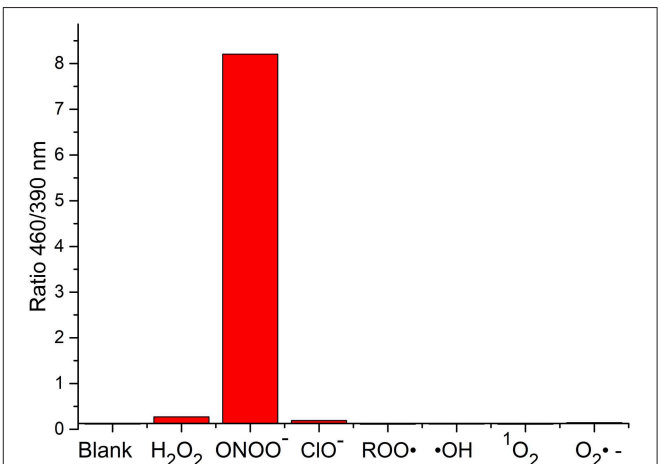

FIGURE 8 | Selectivity data of **5** (10 μM) in the presence of $ONOO^-$ (20 μM), H_2O_2 (100 μM), ClO^- (100 μM), ROO· (100 μM), OH (100 μM), $O_2^{\bullet-}$ (100 μM), and $^1O_2$ (100 μM) in PBS buffer pH = 7.3. The data was collected at 25°C after incubation for 15 min, where λ_{ex} = 345 (16 bandwidth) nm. Fluorescence intensity points were taken at λ_{max} = 460/390 nm.

spectrum the probes have an initial absorption maximum at 315 nm. On addition of $ONOO^-$, the absorption maximum shifts to 360 nm. The redox regulated response was monitored by subjecting 10 μM of each probe, **CC-RNS** and **CI-RNS**, to increasing concentrations of the biological oxidant $ONOO^-$. **Figures 5**, **6** shows that initially both probes are non-fluorescent. There is a strong increase in emission at 460 nm for both probes; ca. **22**- fold for **CI-RNS** and **33-fold** for **CC-RNS** with increasing concentrations of $ONOO^-$ (0–50 μM and 0–30 μM, respectively). The limit of detection (LOD) for **CC-RNS** is 0.29 μM and 37.2 μM for **CI-RNS** (**Supplementary Figures 11–14**).

The process of RNS triggered release of coumarin from **CC-RNS** and **CI-RNS** was supported by mass spectrometric evaluation. The experiments determined that $[M]^-$ =192.0438 and $[M]^+$ = 192.0387 for **CC-RNS** and **CI-RNS**, respectively (**Supplementary Figures 15, 16**). This mass corresponds to formation of compound **4**; the expected cleavage product of the reaction. The formation of free coumarin demonstrates that these systems do release the drug payload *in situ*.

The change in fluorescent properties of potential theranostics **CC-RNS**, **CI-RNS**, probes **5** and **6** were investigated in the presence of various biologically relevant ROS; hydrogen peroxide (H_2O_2), hypochlorite (ClO^-), superoxide ($O_2^{-\bullet}$), singlet oxygen ($^1O_2$), hydroxyl radical (HO•), and peroxyl radical (ROO•). Pleasingly, **CC-RNS**, **CI-RNS**, **5** and **6** are highly selective toward $ONOO^-$ (**Figures 7–9**, **Supplementary Figures 17–20**).

After confirming the selectivity and sensitivity of **CC-RNS** and **CI-RNS** for $ONOO^-$, we evaluated the reaction of **CC-RNS** and **CI-RNS** with $ONOO^-$ in cells. HeLa (cervical cancer) cells were pre-treated with **CI-RNS** or **CC-RNS**. Subsequently, SIN-1 (an $ONOO^-$ donor) was added to produce intracellular $ONOO^-$. As shown in **Figure 10**, the probe alone resulted in a weak fluorescence in cells. However, treatment with SIN-1 led to a significant increase in the fluorescence intensity enabling the visualization of $ONOO^-$ in living cells. Cytotoxicity studies for both **CC-RNS** and **CI-RNS** indicate that the probes are almost non-toxic to Hela cells after incubation with SIN-1 and illumination (ESI-**Supplementary Figures 21, 22**). Hence, no further imaging studies were undertaken.

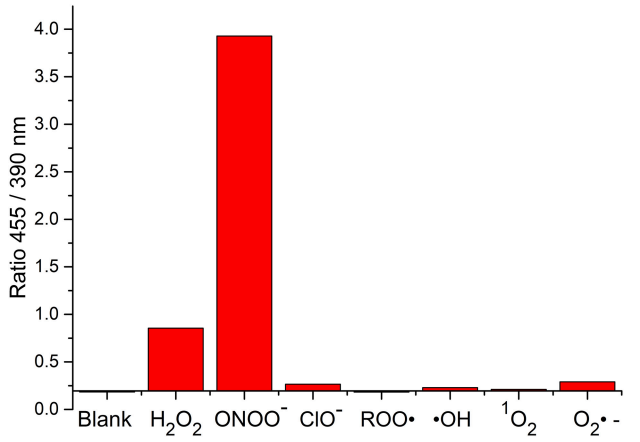

FIGURE 9 | Selectivity data of **6** (10 μM) in the presence of $ONOO^-$ (20 μM), H_2O_2 (100 μM), ClO^- (100 μM), ROO· (100 μM), ·OH (100 μM), $O_2^{\bullet -}$ (100 μM), and $^1O_2$ (100 μM) in PBS buffer pH = 7.3. The data was collected at 25°C after incubation for 15 min, where λ_{ex} = 345 (16 bandwidth) nm. Fluorescence intensity points were taken at λ_{max} = 455/390 nm.

CONCLUSION

In this work, we have developed two novel drug conjugate systems, **CC-RNS** and **CI-RNS**. The drug conjugate systems were designed to integrate a Shabat-based "coumarin linker" with an $ONOO^-$ trigger. The systems incorporated the therapeutics drug payloads of chlorambucil and indomethacin as esters for potential theranostic application. Pleasingly, for each system *in solution*, the probes displayed a selective turn-on response toward $ONOO^-$. In addition, *in vitro* evaluation with HeLa cells demonstrated that the probes were able to successfully visualize endogenous $ONOO^-$ production, providing a potential platform to be able to monitor $ONOO^-$ mediated drug release in cancer cell lines.

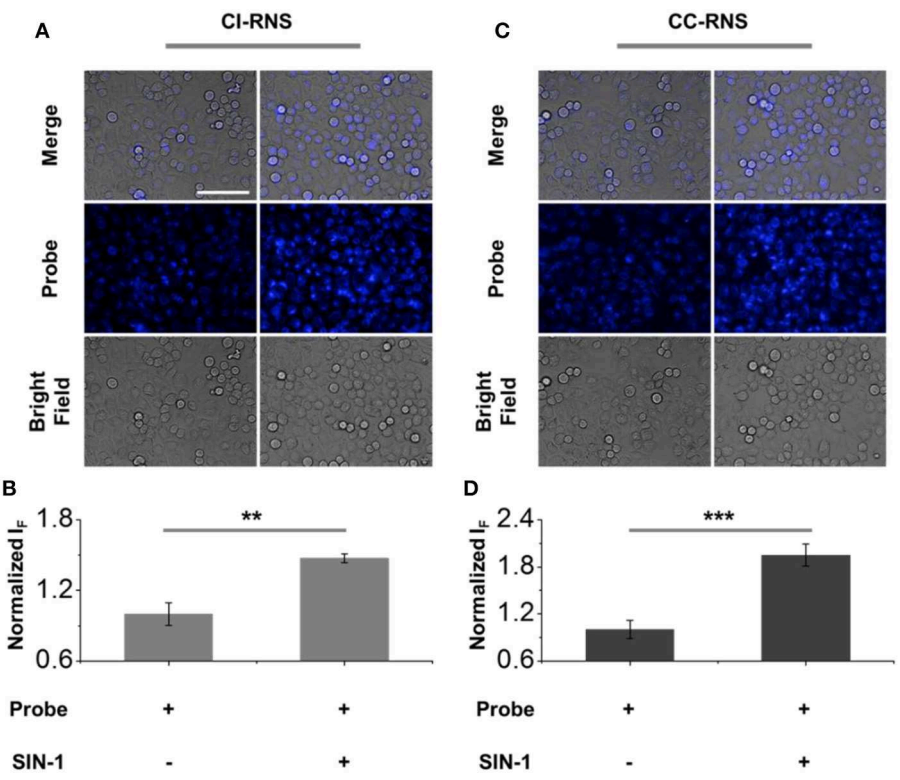

FIGURE 10 | Fluorescence imaging and quantification of **(A,B) CI-RNS** (20 μM) and **(C,D) CC-RNS** (20 μM) in the presence of SIN-1 (500 μM) of HeLa cells. Excitation channel 360–400 nm, emission channel filtered = 410–480 nm. Scale bar = 100 μm. $^{**}P < 0.01$; $^{***}P < 0.001$.

We are currently working on the development of longer wavelength "fluorophore linkers" using ester attachments to appropriate therapeutic units that will facilitate the use of such probes in an animal model in order to evaluate their therapeutic value.

DATA AVAILABILITY STATEMENT

All datasets generated for this study are included in the article/**Supplementary Material**.

AUTHOR CONTRIBUTIONS

AS originated the idea and developed the synthetic route. JG and MO carried out synthesis. MO performed fluorescence experiments. H-HH carried out cell imaging studies under supervision from X-PH. MO wrote the manuscript with the support of SB and TJ. All authors read and approved the final manuscripts.

ACKNOWLEDGMENTS

We would like to thank the EPSRC and the University of Bath for funding. TJ wishes to thank the Royal Society for a Wolfson Research Merit Award. MO, JG, and AS thank the EPSRC for their studentships. X-PH wishes to thank the National Natural Science Foundation of China (21722801), the Science and Technology Commission of Shanghai Municipality (15540723800) and the Shanghai Rising-Star Program (16QA1401400) for financial support. Characterization facilities were provided through the Material and Chemical Characterization Facility (MC^2) at the University of Bath (http://go.bath.ac.uk/mc2). All data supporting this study are provided as **Supplementary Information** accompanying this paper.

SUPPLEMENTARY MATERIAL

The Supplementary Material for this article can be found online at: https://www.frontiersin.org/articles/10.3389/fchem.2019.00775/full#supplementary-material

REFERENCES

Ackerstaff, E., Gimi, B., Artemov, D., and Bhujwalla, Z. M. (2007). Anti-inflammatory agent indomethacin reduces invasion and alters metabolism in a human breast cancer cell line. *Neoplasia* 9, 222–235. doi: 10.1593/neo.06673

Aulic, S., Bolognesi, M. L., and Legname, G. (2013). Small-molecule theranostic probes: a promising future in neurodegenerative diseases. *Int. J. Cell Biol*. 2013, 1–19. doi: 10.1155/2013/150952

Beckman, J. S. (1996). "The physiological and pathological chemistry of nitric oxide," in *Nitric Oxide: Principles and Actions*, eds J. R. Lancaster. Orlando, FL: Academic, 1–82. doi: 10.1016/B978-012435555-2/50002-4

Begleiter, A., Mowat, M., Israels, L. G., and Johnston, J. B. (1996). Chlorambucil in chronic lymphocytic leukemia: mechanism of action. *Leuk. Lymphoma.* 23, 187–201. doi: 10.3109/10428199609054821

Behara, K. K., Rajesh, Y., Venkatesh, Y., Pinninti, B. R., Mandal, M., and Singh, N. D. P. (2017). Cascade photocaging of diazeniumdiolate: a novel strategy for one and two photon triggered uncaging with real time reporting. *Chem. Commun*. 53, 9470–9473. doi: 10.1039/C7CC04635A

Blau, R., Epshtein, Y., Pisarevsky, E., Tiram, G., Dangoor, S. I., Yeini, E., et al. (2018). Image-guided surgery using near-infrared Turn-ON fluorescent nanoprobes for precise detection of tumor margins. *Theranostics* 8, 3437–3460. doi: 10.7150/thno.23853

Borges, F., Roleira, F., Milhazes, N., Santana, L., and Uriarte, E. (2005). Simple coumarins and analogues in medicinal chemistry: occurrence, synthesis and biological activity. *Curr. Med. Chem*. 12, 887–916. doi: 10.2174/0929867053507315

Chan, J., Dodani, S. C., and Chang, C. J. (2012). Reaction-based small-molecule fluorescent probes for chemoselective bioimaging. *Nat. Chem*. 4, 973–984. doi: 10.1038/nchem.1500

Gangopadhyay, M., Mengji, R., Paul, A., Venkatesh, Y., Vangala, V., Jana, A., et al. (2017). Redox-responsive xanthene-coumarin-chlorambucil-based FRET-guided theranostics for "activatable" combination therapy with real-time monitoring. *Chem. Commun*. 53, 9109–9112. doi: 10.1039/C7CC03241B

Guo, Y. C., Chang, C. M., Hsu, W. L., Chiu, S. J., Tsai, Y. T., Chou, Y. H., et al. (2013). Indomethacin inhibits cancer cell migration via attenuation of cellular calcium mobilization. *Molecules* 18, 6584–6596. doi: 10.3390/molecules18066584

Kaur, J., Tsvetkova, Y., Arroub, K., Sahnoun, S., Kiessling, F., and Mathur, S. (2017). Synthesis, characterization, and relaxation studies of Gd-DO3A conjugate of chlorambucil as a potential theranostic agent. *Chem. Biol. Drug. Des*. 89, 269–276. doi: 10.1111/cbdd.12827

Kim, E. J., Bhuniya, S., Lee, H., Kim, H. M., Cheong, C., Maiti, S., et al. (2014). An activatable prodrug for the treatment of metastatic tumors. *J. Am. Chem. Soc*. 136, 13888–13894. doi: 10.1021/ja5077684

Kumar, R., Han, J., Lim, H.-J., Ren, W. X., Lim, J.-Y., Kim, J.-H., et al. (2014). Mitochondrial induced and self-monitored intrinsic apoptosis by antitumor theranostic prodrug*: in vivo* imaging and precise cancer treatment. *J. Am. Chem. Soc*. 136, 17836–17843. doi: 10.1021/ja510421q

Kumar, R., Kim, E. J., Han, J., Lee, H., Shin, W. S., Kim, H. M., et al. (2016). Hypoxia-directed and activated theranostic agent: imaging and treatment of solid tumor. *Biomaterials* 104, 119–128. doi: 10.1016/j.biomaterials.2016.07.010

Kumar, R., Shin, W. S., Sunwoo, K., Kim, W. Y., Koo, S., Bhuniya, S., et al. (2015). Small conjugate-based theranostic agents: an encouraging approach for cancer therapy. *Chem. Soc. Rev*. 44, 6670–6683. doi: 10.1039/C5CS00224A

Lu, S. C. (2013). Glutathione synthesis. *Biochim. Biophys. Acta Gen. Subj*. 1830, 3143–3153. doi: 10.1016/j.bbagen.2012.09.008

Lucas, S. (2016). The pharmacology of indomethacin. *Headache* 56, 436–446. doi: 10.1111/head.12769

Millard, M., Gallagher, J. D., Olenyuk, B. Z., and Neamati, N. (2013). A selective mitochondrial-targeted chlorambucil with remarkable cytotoxicity in breast and pancreatic cancers. *J. Med. Chem*. 56, 9170–9179. doi: 10.1021/jm4012438

Miller, E. W., Albers, A. E., Pralle, A., Isacoff, E. Y., and Chang, C. J. (2005). Boronate-based fluorescent probe for imaging cellular hydrogen peroxide. *J. Am. Chem. Soc*. 127, 16652–16659. doi: 10.1021/ja054474f

Pacher, P., Beckman, J. S., and Liaudet, L. (2007). Nitric oxide and peroxynitrite in health and disease. *Physiol. Rev*. 87, 315–424. doi: 10.1152/physrev.00029.2006

Sedgwick, A. C., Han, H.-H., Gardiner, J. E., Bull, S. D., He, X.-P., and James, T. D. (2018). The development of a novel AND logic-based fluorescence probe for the detection of peroxynitrite and GSH. *Chem. Sci*. 9, 3672–3676. doi: 10.1039/C8SC00733K

Sedgwick, A. C., Han, H. H., Gardiner, J. E., Bull, S. D., He, X. P., and James, T. D. (2017). Long-wavelength fluorescent boronate probes for the detection and intracellular imaging of peroxynitrite. *Chem. Commun*. 53, 12822–12825. doi: 10.1039/C7CC07845E

Sedgwick, A. C., Sun, X. L., Kim, G., Yoon, J., Bull, S. D., and James, T. D. (2016). Boronate based fluorescence (ESIPT) probe for peroxynitrite. *Chem. Commun*. 52, 12350–12350. doi: 10.1039/C6CC06829D

Thasnim, P., and Bahulayan, D. (2017). Click-on fluorescent triazolyl coumarin peptidomimetics as inhibitors of human breast cancer cell line MCF-7. *New J. Chem*. 41, 13483–13489. doi: 10.1039/C7NJ02712E

Wang, Q. Q., Begum, R. A., Day, V. W., and Bowman-James, K. (2010). Sulfur, oxygen, and nitrogen mustards: stability and reactivity. *Org. Biomol. Chem*. 10, 8786–8793. doi: 10.1039/c2ob26482j

Wang,. C.-K., Cheng, J., Liang, X.-G., Tan, C., Jiang, Q., Hu, Y.-Z., et al. (2017). A H_2O_2-responsive theranostic probe for endothelial injury imaging and protection. *Theranostics* 7, 3803–3813. doi: 10.7150/thno.21068

Weber, M., Mackenzie, A. B., Bull, S. D., and James, T. D. (2018). Fluorescence based tool to detect endogenous peroxynitrite in M1-polarised murine J774.2 macrophages. *Anal. Chem*. 90, 10621–10627. doi: 10.1021/acs.analchem.8b03035

Weinstain, R., Segal, E., Satchi-Fainaro, R., and Shabat, D. (2013). Real-time monitoring of drug release. *Chem. Commun*. 46, 553–555. doi: 10.1039/B919329D

Wu, L. L., Wang, Y., Weber, M., Liu, L. Y., Sedgwick, A. C., Bull, S. D., et al. (2018). ESIPT-based ratiometric fluorescence probe for the intracellular imaging of peroxynitrite. *Chem. Commun*. 54, 9953–9956. doi: 10.1039/C8CC04919J

Wu, X., Sun, X., Guo, Z., Tang, J., Shen, Y., James, T. D., et al. (2014). *In vivo* and *in situ* tracking cancer chemotherapy by highly photostable NIR fluorescent theranostic prodrug. *J. Am. Chem. Soc*. 136, 3579–3588. doi: 10.1021/ja412380j

Yang, D., Wang, H.-L., Sun, Z.-N., Chung, N.-W., and Shen, J.-G. (2006). A highly selective fluorescent probe for the detection and imaging of peroxynitrite in living cells. *J. Am. Chem. Soc*. 128, 6004–6015. doi: 10.1021/ja0603756

Yang, Y. F., Xu, W., Song, W., Ye, M., and Yang, X. W. (2015). Transport of twelve coumarins from angelicae pubescentis radix across a MDCK-pHaMDR cell monolayer-an *in vitro* model for blood-brain barrier permeability. *Molecules* 20, 11719–11732. doi: 10.3390/molecules200711719

Conflict of Interest: The authors declare that the research was conducted in the absence of any commercial or financial relationships that could be construed as a potential conflict of interest.